

**LOW TEMPERATURE FERROELECTRIC BEHAVIOR IN
MORPHOTROPIC $\text{Pb}(\text{Zr}_{1-x}\text{Ti}_x)\text{O}_3$**

J. B. J. CHAPMAN*

*Department of Physics and Astronomy, University College London, Gower Street, London
WC1E 6BT, UK*

National Physical Laboratory, Hampton Road, Teddington, TW11 0LW, UK

O. T. GINDELE

*Department of Physics and Astronomy, University College London, Gower Street, London
WC1E 6BT, UK*

National Physical Laboratory, Hampton Road, Teddington, TW11 0LW, UK

C. VECCHINI

National Physical Laboratory, Hampton Road, Teddington, TW11 0LW, UK

P. THOMPSON

XMaS, The UK-CRG, ESRF, BP 220, F-38043 Grenoble CEDEX, France

Department of Physics, University of Liverpool, Liverpool, L69 3BX, UK

M. STEWART

National Physical Laboratory, Hampton Road, Teddington, TW11 0LW, UK

M. G. CAIN

Electrosiences Ltd, 1 Osborn Road, Farnham, GU9 9QT, UK

D. M. DUFFY

*Department of Physics and Astronomy, University College London, Gower Street, London
WC1E 6BT, UK*

A. KIMMEL

*Department of Physics and Astronomy, University College London, Gower Street, London
WC1E 6BT, UK*

ABSTRACT. We provide an insight into the switching of near-morphotropic composition of PZT using molecular dynamics simulations and electrical measurements. The simulations and experiments exhibit qualitatively similar hysteretic behavior of the polarization for different temperatures showing widening of the P-E loops and the decrease of the coercive field towards high T. Remarkably, we have shown that polarization switching at low temperatures occurs via polarization rotation, that is a fundamentally different mechanism from high temperature switching, which is nucleation driven.

1. INTRODUCTION

Functional ferroelectric ceramics are utilized as critical components in many modern technologies which operate over a wide range of conditions. One of the most widely used ceramic materials is lead zirconate titanate $\text{Pb}(\text{Zr}_{1-x}\text{Ti}_x)\text{O}_3$ (PZT)¹, which is a disordered solid solution of PbTiO_3 and PbZrO_3 perovskite (ABX_3) compounds^{2,3,4,5,1,6,7} used for non-volatile

memories, transducers, actuators, inkjet printheads, drug delivery implants and micropumps^{8,9}. The permutational freedom resulting from the random distribution of Ti and Zr over the B-sites unlocks rotational degrees of freedom of the BO_6 octahedra which provides a rich temperature-composition phase diagram. Of particular importance is the morphotropic region around $0.47 < x < 0.52$, which exhibits exceptionally high electromechanical response vital for aeronautical, military and space applications^{10,11,12}. It is essential to provide insight into the performance and polarization switching dynamics of this material due to the wide range of operating conditions of PZT based devices. Although there have been a number of studies performed at room temperature and above, the low temperature ($T < 200$ K) properties of PZT are not well characterized.

In this work we study the temperature effect on electromechanical properties of PZT and provide insight into the switching mechanisms at different temperatures. In order to investigate the effect of temperature on the important properties of PZT we have carried out a series of classical molecular dynamics (MD) simulations and also electrical measurements of P-E loops in ceramic PZT ($x=0.47$) samples. We employed large scale MD simulations to calculate hysteresis (P-E) loops for the PZT compound over a wide range of temperatures, which provides information about both the local polarization in each unit cell and the macroscopic polarization. Although P-E loops in PZT for different temperatures have been measured experimentally before¹³, the temperature dependence of the coercive field (E_C) and its implications have not been discussed.

2. SIMULATION AND EXPERIMENTAL PROCEDURE

2.1. Simulation Details. We used an adiabatic core-shell model forcefield, that accurately reproduces the full composition-temperature phase diagram for PZT for our simulations⁴. A relatively large simulation cell of $\text{PbZr}_{0.5}\text{Ti}_{0.5}\text{O}_3$ was used ($20 \times 20 \times 20$ unit cells) corresponding to 4×10^4 atoms. The two species of B-cations (Ti and Zr) were randomly distributed over the B-sites to obtain the stoichiometry of $\text{PbZr}_{0.5}\text{Ti}_{0.5}\text{O}_3$. We employed the DL_POLY_4¹⁴ code with the $N\sigma T$ (constant strain) ensemble and a Nosé-Hoover thermostat (0.01 ps) and barostat (0.1 ps). A time step of 0.2 fs was selected. In this model, to incorporate the polarizability of the atoms, the widely-used adiabatic approach is employed whereby each

atom is comprised of two charged particles: a massive core and a light shell tethered by an isotropic anharmonic spring potential. Assigning a fraction of the mass to the shell enables a dynamical description of both the core and shell¹⁵. A mass of 7 amu is applied to the Pb, Ti and Zr shells and 2 amu to the O shells, sufficiently light to reproduce correct polarizations and phases but massive enough to ensure the natural frequency of vibration of the spring far exceeds the vibrational frequency of the atom. The Smooth Particle Mesh Ewald (SPME) summation method is used to calculate the electrostatic interactions between the cores and shells of different atoms. Short range interactions are described by Buckingham potentials. Full details regarding the forcefield parameters are as shown in⁴. For the parent compound PbTiO_3 , this model reproduces the Born effective charge tensors, the elastic properties, $c(2 \times 2)$ surface reconstructions, thin film domain morphologies and soft phonon modes in excellent agreement with density functional theory (DFT) calculations^{4,16}.

We performed quasistatic P-E loop calculations by ramping the electric field along [001] in 1 MV/m steps in a range from -30 MV/m to +30 MV/m. The system was equilibrated for 4 ps at each value of the electric field and the polarization was calculated during a subsequent production run of 6 ps. The calculation of the local polarization was performed using the method of Sepiarsky and Cohen¹⁷. Further details of the polarization calculation are provided in the Supplementary Information.

2.2. Experimental Details. For comparison with the theoretical predictions of the P-E loop behavior we performed electrical measurements of ceramic PZT samples ($x=0.47$). The measurements were performed on the XMaS beam-line (BM28) at the European Synchrotron Radiation Facility (ESRF), where we used a method to measure P-E loops on the beam-line which has been previously described in¹⁸, that we label setup 1, and at NPL using a liquid nitrogen bath for the 77K data point observed in Fig. 1b, which we label setup 2. P-E loops were measured in setup 1 on commercial ceramic plates of soft PZT by Morgan Electroceramics (PC5H). Earlier reports found the material's composition to be $x=0.47$ with a rhombohedral symmetry at room temperature¹⁹. This places the composition at the MPB, at which a more recent neutron scattering study suggests¹ that an additional monoclinic phase coexists with the rhombohedral phase. A separate measurement point at 77K was made in liquid nitrogen

using a Fuji c91 (PZT composition similar to Morgan’s PC5H) sample that permitted higher electric fields to be applied. To measure the P-E loops, triangular electric field cycles of amplitude 1 kV/mm and a frequency of 0.1 Hz were applied to the device under test, while the polarization was recorded simultaneously. Further details about the experimental setup are provided in the Supplementary Information.

3. RESULTS

3.1. Simulations. Our P-E loop simulations for $\text{PbZr}_{0.5}\text{Ti}_{0.5}\text{O}_3$ (Fig. 1a) produce symmetric, well-saturated square-shaped loops characteristic of a hard ferroelectric system. As the temperature increases, the P-E loops become narrower and exhibit a more complex shape, signifying that the switching process occurs via a series of multiple events activated across a broader range of fields²⁰. Above 300 K the shape of P-E loops becomes more complex because of increasing polarization fluctuations in the system. At high temperatures a small amount of in-plane polarization along x and y develops spontaneously, which reduces the z -component (P_Z), whilst the total polarization is unchanged. We obtained the value of E_C and P_S from the P-E loops. The temperature behavior of P_S shows a monotonic increase, while E_C decreases with the temperature rise (Fig. 1b). Thus, at low temperatures (< 200 K) the values of E_C exceed the fields of several kV/mm usually applied in experiments and devices. The implication of this increase is that high fields are necessary for ferroelectric devices at low temperatures.

3.2. Experiments. The experimental P-E curves (Fig. 1c) display the expected hysteretic behavior with dielectric loss determined by the area enclosed within the P-E loop. Cooling the sample from room temperature to 250 K shows a slight increase of E_C . Further lowering of the temperature to 200 K is accompanied by a widening of the P-E loop that results in a lower P_S and an increase in E_C . This is in good qualitative agreement with our simulations and typical for ferroelectric materials, as shown earlier for PZT¹³, BiFeO_3 ²¹, $\text{SrBi}_2\text{Ta}_2\text{O}_9$ ²² and ferroelectric polymers²³. Upon further cooling, we observed that at temperatures below 160 K the P-E loops exhibit a very narrow hysteresis and low polarization, akin to curves of lossy dielectrics. This is similar to observations made from measurements of PZT in an earlier NASA report¹³. The narrow loops and low coercive fields observed at low temperature in our

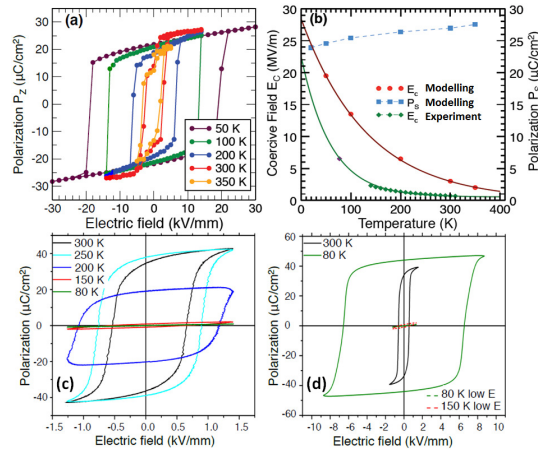


FIGURE 1. (a) Modelled temperature dependence of the z -component of polarization (P_z) with respect to the applied electric field E (P-E loops). With the temperature rise, the shape of P-E loops evolves from square-like (purple, green, blue) to complex shapes (red and yellow) due to increased polarization fluctuation at high temperatures. (b) Temperature dependence of E_C (red) and P_S (blue), both inferred from the P-E loops in (a). E_C drops with temperature (maroon). Experimental data also plotted in green diamonds with one (77K) point in purple diamond (different sample, but same composition). (c) Measured P-E loops of PZT sample at different temperatures. With the temperature decrease the area of the loops reduce, demonstrating a dielectric-like response. (d) A comparison of 150 K and 80 K loops measured at high (9 kV/mm) and low (1.5 kV/mm) fields. The higher 9 kV/mm field restores the square shaped hysteresis loops.

data are a direct result of E_C becoming larger than the maximum applied voltage possible, in the first of our setups, equating to 1.5 kV/mm for the PC5H samples. These non-switching data sets have been left in this paper as an important observation for experimentalists when reporting, sometimes erroneous, low temperature ferroelectric data. Application of high fields of 9 kV/mm (using the much thinner Fuji samples) restores the observation of large square hysteresis loops as shown in Fig. 1d - labelled 300 K and 80 K data.

4. DISCUSSION

Our electrical measurement of PZT ceramics and single domain modelling results demonstrate good qualitative agreement. This behavior highlights the importance of temperature on measured material properties, where a small change of temperature strongly affects E_C and related quantities. However, we found quantitative differences between the modelled and experimental parameters. Indeed, the E_C in experiments is less than half that found in

MD simulations. We assume that the lower value measured in the experiments is due to the presence of domain walls, defects, grain boundaries and surface terminations in the ceramic samples. Inhomogeneity in the local polarization introduce the possibility of switching via domain wall motion, which reduces the switching barrier. Indeed, for the parent compound PbTiO_3 , the coercive field as calculated from the forcefield at 10 K is 130 kV/mm²⁴ which matches other PbTiO_3 MD parametrizations²⁵ and is in excellent agreement with the intrinsic coercive field of 150 kV/mm calculated using density functional perturbation theory²⁶.

To further validate the results of the forcefield for morphotropic PZT we calculate the 180° and 90° domain wall energy using large scale MD and compare with density functional theory calculations (full details on the procedure and results are provided in the Supplementary Information). The domain wall energies calculated for 180° domains are in excellent agreement having a converged value of 130 mJ/m² calculated from both MD and DFT. This value is comparable to pure PbTiO_3 reported to have a domain wall energy of 130 mJ/m²²⁷ and the 160 mJ/m² for Zr centred domain walls in rocksalt PZT²⁸. For 90° domain walls the forcefield and DFT calculations show weaker agreement, finding 43 mJ/m² and 29 mJ/m² respectively. The forcefield overestimates the 90° domain wall energy by a factor of two as is similarly observed by other shell-model forcefields for Pb based ferroelectrics²⁹ but notably is very close to experimental observations of 50 mJ/m²³⁰.

We found that the E_C in Fig. 1b is about an order of magnitude lower than the E_C value calculated from first-principles for switching through the polar ferroelectric mode in PZT by Beckman et al²⁸. The lower E_C found in our model, fitted to DFT data which has the large repolarization barrier⁴, suggests that the actual polarization switching in PZT follows a lower energy path than the polar mode. Two intrinsic mechanisms that could lower the repolarization barrier are polarization rotation and domain wall motion after domain nucleation³¹.

4.1. Switching Dynamics. To understand the origin of the low values of E_C and provide an insight into the switching mechanisms in the different temperature regimes we have modelled the switching events using molecular dynamics at 100 K and 300 K. We initially pre-pole the system with an electric field along [001] such as that we induce a tetragonal phase with $P_z =$

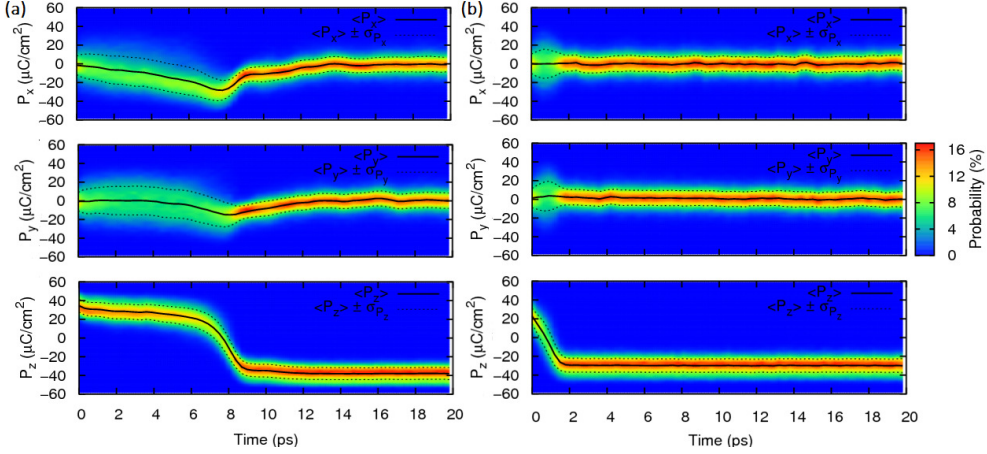


FIGURE 2. Behavior of the local order parameter polarization during switching at (a) 100 K and (b) 300 K. The solid black lines trace the mean of the i^{th} polarization component $\langle P_i \rangle$. Dotted lines trace the standard deviation from the mean displacement $\langle P_i \rangle \pm \sigma_{P_i}$. Sign change of $\langle P_z \rangle$ indicates different switching times of 8 ps for 100 K and 2 ps for 300 K. At 100 K the reduction of P_z is accompanied by substantial deviations in the P_x and P_y components which corresponds to maintained polarization rotation. In contrast, at 300 K the P_z component changes the sign, while the in-plane components of polarization remains, on average, zero.

$40 \mu\text{C}/\text{cm}^2$ and $P_x = P_y \approx 0 \mu\text{C}/\text{cm}^2$. We note our forcefield supports a macroscopic electric field driven transformation path of $\text{R} \rightarrow \text{M}_A \rightarrow \text{T}$ as is observed experimentally for morphotropic PZT³² (Supplementary Figure S2, $\text{R}=[111]$; $\text{M}_A=[\nu, \nu, 1]$, $0 < \nu < 1$; $\text{T}=[001]$). A reverse field of magnitude 30 MV/m was applied along $[00\bar{1}]$ to facilitate picosecond switching at the start of the production run. To characterize the switching dynamics we register the time evolution of the free energy, following the definition given in ref.³³. The free energy expressed as a Density of Probability (DoP) is defined as the mean of the order parameter, which here returns the averaged local polarization (Figure 2). We plot the evolution of order parameters and DoP in Figure 2 where the vertical axis represents the polarization and the colour gradient reflects the proportion of unit cells having a given polarization at all instances of the simulation^{34,33}. The free energy profile is further characterized by the standard deviation of the order parameter.

We have registered different switching times of 8 ps and 2 ps for the 100 K and 300 K simulations, respectively, identified by $\langle P_z \rangle$ changing sign. This behavior agrees well with experiments on PZT ceramics which identified decreased switching times with increasing temperature³⁵.

Remarkably, we observed a stark contrast between the DoP for low and room temperature regimes. At 300 K the average P_Z component changes the sign, whilst the average in-plane components of polarization remains zero (Fig. 2b). This corresponds to the simulated sample switching through an intermediate quasi-paraelectric state (Figure 2b). In contrast, at 100 K, the reduction in the average polarization parallel to the switching field is accompanied by substantial build up in the P_x and P_y components showing polarization rotation to within a standard deviation (Figure 2a). A similar switching mechanism has been described in MD simulations of tetragonal PbTiO_3 in which the system switched via an intermediate orthorhombic phase²⁵ and supports experimentally observed double current peaks in pre-poled PZT identifying non-180° switching³⁶. We note that for the low temperatures case the standard deviation in $P_{x,y}$ slightly increases during the switching event, which is indicative of bond softening³⁴ and the remnants of the competing rotational mechanism. At the higher temperature the system responded to the applied field by nucleation of small reversed domains that can switch rapidly. This prevents the build up of large polarization components perpendicular to the driving field and reduces the time and energy required for polarization reversal, resulting in slanted hysteresis loops.

4.2. Switching Mechanisms. The nucleation dominated switching at 300 K agrees well with experimental findings for thin PZT films³⁷, where it was proposed that at room temperature PZT re-poles through multiple nucleation events, while at lower temperatures domain wall motion dominates the switching kinetics. Here we suggest that, in the absence of domain walls, polarization rotation initiates the low temperature switching. We emphasize the difference between switching at low and room temperature in Fig. 3, where we present a schematic sketch together with snapshots of the simulated PZT system at 100 K and 300 K. The snapshots are plotted as 2D slices in the x-z plane in (b) and (c), demonstrating the distinctly different domain structures related to each switching process. The figures of the modelled system show the local dipole moments, for the system switching from P_Z to $-P_Z$ at the state where $P_Z = 0$, halfway through the polarization reversal ($t(\text{b})=7.9$ ps, $t(\text{c})=0.85$ ps). One can see that at 100 K (Fig. 3b) the system consists of large domains with significant in-plane polarization and $P_Z \sim 0$. This agrees with Fig. 2a, which shows a large contribution of the

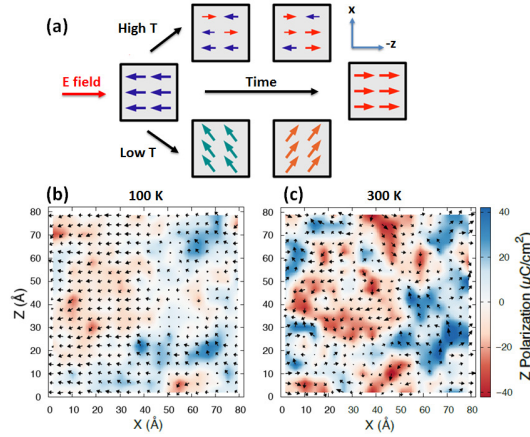


FIGURE 3. (a) Schematic representation of the different polarization switching mechanisms: Polarization rotation at lower temperature (left) and nucleation of reversed domains at higher temperature (right). The arrows correspond to the local dipole moments. (b) and (c) Snapshots of the local dipoles in PZT during MD simulated polarization switching at 100 K and at 300 K. The snapshots were taken halfway through the polarization reversal (total $P_Z = 0$) and each arrow corresponds to the local dipole moment of a conventional unit cell. The colour gradient represents the magnitude of P_Z . (b) The low temperature system ($T=100$ K) exhibits a homogeneous domain pattern during the switching process with well-defined in-plane contribution where P_Z is small and P_X is large. (c) At high temperature ($T=300$ K) PZT breaks up into multiple reversed domains, as seen by the many up (blue) and down (red) polarized parts.

x -component of polarization during the switching. In contrast, the system at 300 K (Fig. 3c) exhibits a much denser domain pattern with small domains polarized along $+z$ or $-z$ and much less in-plane polarization along x . Overall, the 100 K domain structure is more homogeneous than the 300 K domain structure.

Using the local polarization we plot the domain structure that nucleates and grows via domain wall motion in the low temperature simulation (Figure 4). Each conventional unit cell is represented by a cube whose colour indicates the local phase adopted by the cell. Phases of the unit cells are defined by the average polarization \bar{P} of the cell over 50 fs increments. Following the approach from³⁴, if $\bar{P} < 5 \mu\text{C}/\text{cm}^2$ the unit cell is considered non-polar and cubic (C). If a component of \bar{P} exceeds $5/\sqrt{6} \mu\text{C}/\text{cm}^2$ then it is classed as ferroelectric. The phase is then identified by the number of components exceeding this limit ($T=1, O=2, R=3$). An x - z cross-section is taken at 1 ps (Fig. 4a) and 6 ps (Fig. 4b), and cartoons depicting both phase structures are shown in Figure 4(ii). Only switched unit cells ($P_z^j < 0$) are plotted.

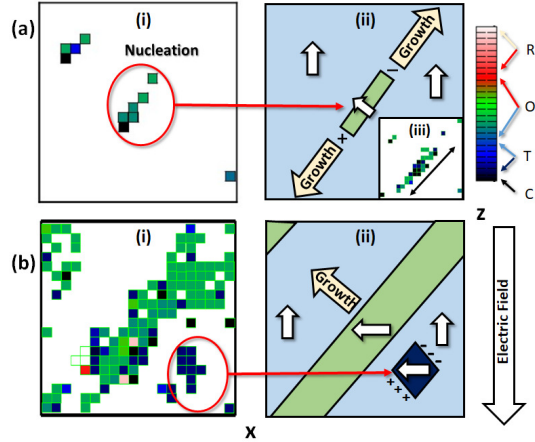


FIGURE 4. Low temperature switching mechanism of forward poled $\text{PbZr}_{0.5}\text{Ti}_{0.5}\text{O}_3$. Snapshots at (a) 1 ps and (b) 6 ps during the switching simulation at 100 K. (i) Negatively poled unit cells are plotted whose colour represents the local phase. (ii) Simplified cartoons of the snapshots.

When the switching field is applied to the system, in which pre-existing domain walls are absent, octahedral shaped reverse domains are nucleated, approximately faceted by (101) surfaces (Fig. 4a). These are the 3-dimensional analogues to the bevelled diamond formations previously identified to be the shape which minimizes the nucleation barrier on 2-dimensional 180° domain walls during domain wall motion³¹. We find that nuclei exceeding some critical radius with this structure quickly grow on the facets that form charged domain walls with the [001] bulk, which tends to reduce the electrostatic energy penalty (Fig. 4a(iii)). This growth is followed by conventional domain wall motion (Fig. 4b). This nucleated domain accounts for the polarization rotation observed in Figure 2a, as the local unit cells within the reverse domain adopt an orthorhombic structure with the polarization rotating as the domain grows. In order to investigate finite size effects we repeated the 100 K simulation for a $60 \times 20 \times 60$ simulation cell containing 3.4×10^5 atoms which shows similar polarization rotation during switching (see supplementary Figure S3).

At both low and room temperatures the underlying domain structures affect the macroscopic lattice parameters and reduce the tetragonality of the forward poled system during the switching event (Figure 5 a & b). The uncorrelated nature of the small nucleated domains at room temperature results in an intermediate macroscopic cubic structure, whereas at low temperature the lattice parameters reflect the growth of the rotating domain. In Figure 5 c

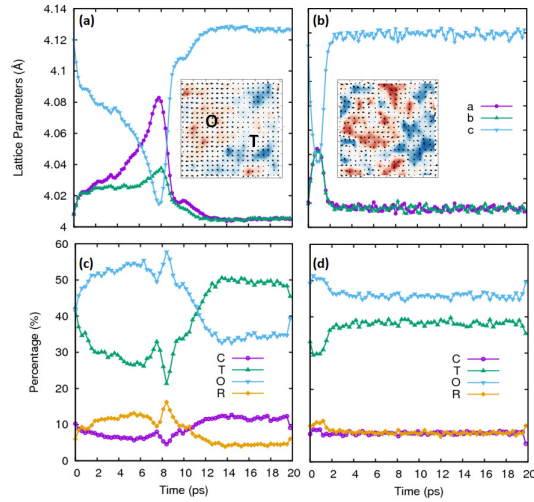


FIGURE 5. Average lattice parameters during the switching event at (a) 100 K and (b) 300 K. Proportion of the local unit cells having cubic, tetragonal, orthorhombic and rhombohedral phases during the simulation at (a) 100 K and (b) 300 K. Phases of the unit cells are defined by the average polarization \bar{P} of the cell over 50 fs increments. In an approach from³⁴, if $\bar{P} < 5 \mu\text{C}/\text{cm}^2$ the unit cell is considered non-polar and cubic (C). If a component of \bar{P} exceeds $5/\sqrt{6} \mu\text{C}/\text{cm}^2$ then it is classed as ferroelectric. The phase is then identified by the number of components exceeding this limit (T=1,O=2,R=3).

and d we decompose the system into the proportion of local unit cells supporting C,T,O and R phases at each instant in time. At low temperatures, as the nucleated domain grows, the unit cells become orthorhombic as was shown by Figure 4 and by the density of probability of the polarization (Figure 2a). Once the domain has grown and fully rotated the predominantly tetragonal local phase is restored. At room temperature there is again a spike in the percentage of locally orthorhombic cells (Fig. 5d) reflecting the bond softening and remnants of the low temperature switching mechanism. However, these small nucleated domains are uncorrelated, showing the different nature of the two switching types.

Note that, at zero field the forcefield supports the multiple phases of $\text{PbZr}_{0.5}\text{Ti}_{0.5}\text{O}_3$: monoclinic symmetry at 100 K, rhombohedral symmetry at 200 K and tetragonal symmetry at 300 K (see Figure 2c in⁴). The monoclinic and rhombohedral phases could, therefore, be the origin of the the observed rotational mode, by facilitating the polarization rotation. To rule out the correlation of the rotational switching mode with the low temperature symmetries, we modelled a strictly tetragonal PZT composition. We carried out similar calculations of polarization switching events for tetragonal $P4mm$ $\text{PbZr}_{0.2}\text{Ti}_{0.8}\text{O}_3$ at a field of 80 MV/m.

Remarkably, we found that at low temperatures (100 K) the tetragonal $\text{PbZr}_{0.2}\text{Ti}_{0.8}\text{O}_3$ also exhibits rotational polarization switching despite the temperature driven phase transition having only a tetragonal phase below the Curie temperature (see supplementary information).

The observation of two different switching mechanisms at room and low temperatures is indicative of two competing mechanisms that we suggest have different field dependencies of the switching barrier. Vopsaroiu et al³⁸ analysed the temperature and field dependence of the switching time by considering a distribution of barriers. The barrier height falls linearly with applied field due to the linear increase in energy of the unfavorable polarization state. In this model “clusters” of reversed polarization are nucleated in a similar way to³⁹. In the case of PZT, the intrinsic B-site cation disorder will naturally result a distribution of barriers for local clusters, of which those with particularly low barriers would correspond to the nucleation sites identified in³⁸. The polarization rotation switching mechanism would also be expected to have a barrier that decreases linearly with applied field, for the same reason, but the gradient of the decrease would be different. A steeper decrease for the rotation mechanism would ensure that rotation dominates at low temperatures, where the switching fields are higher due to the lower thermal energy. Thus the linear field dependence of the switching barriers could explain the cross-over between mechanisms at low temperature.

5. CONCLUSIONS

Summarising, we have performed classical MD simulations of polarization switching dynamics in near-morphotropic PZT using a shell model force field⁴. We have reproduced the hysteretic behavior of the polarization with applied electric field for different temperatures. The shape of the P-E loops was found to be temperature dependent and exhibits narrowing towards high temperatures. Further, we have shown E_C to increase with decreasing temperature which we confirmed experimentally by electrical measurements. The nature of the switching mechanism, observed from our simulations at room temperature, was in good agreement with earlier experimental studies on PLZT thin films³⁷ where domain nucleation was found to be the dominating switching process. We have shown in this work, however, that at low temperatures the electric-field induced switching of electrical polarization proceeds via the rotation of polarization which has a reduced barrier compared to nucleation driven switching

at larger fields. Our findings provide useful insight into the operational temperature/voltage conditions of ferroelectric-based devices used in aeronautical and space applications.

ACKNOWLEDGEMENTS

The authors are grateful for the fruitful discussions with Prof. R. Cohen and Dr P. Zubko. This work was funded through the European Metrology Research Programme (EMRP) Project IND54 Nanostrain. The EMRP is jointly funded by the EMRP participating countries within EURAMET and the European Union. A.K. acknowledges financial support from the European Unions Horizon2020 research and innovation programme within the PETMEM project (Grant nr. 688282). Via our membership of the UK's HPC Materials Chemistry Consortium, which is funded by EPSRC (EP/L000202), this work made use of the facilities of HECToR and ARCHER, the UK's national high-performance computing service, which is funded by the Office of Science and Technology through EPSRC's High End Computing Programme. J.C. acknowledges financial support from EPSRC (EP/G036675/1) via the Centre for Doctoral Training in Molecular Modelling and Materials Science at University College London.

REFERENCES

1. Zhang, N., Yokota, H., Glazer, A.M., Ren, Z., Keen, D.A., Keeble, D.S., et al. The missing boundary in the phase diagram of $\text{pbzr}_{(1-x)}\text{ti}_x\text{o}_3$. *Nature Communications* 2014; **5**:1–9.
2. Noheda, B., Cox, D.E., Shirane, G., Gonzalo, J.A., Cross, L.E., Park, S.E.. A monoclinic ferroelectric phase in the $\text{pbzr}_{(1-x)}\text{ti}_x\text{o}_3$ solid solution. *Applied Physics Letters* 1999;**74**:2059–2061.
3. Shirane, G., Susuki, K.. Crystal structure of pzt. *Journal of the Physical Society of Japan* 1952;**7**:333–333.
4. Gindele, O., Kimmel, A.V., Cain, M.G., Duffy, D.M.. Shell model force field for lead zirconate titanate $\text{pbzr}_{(1-x)}\text{ti}_x\text{o}_3$. *The Journal of Physical Chemistry C* 2015;**119**:17784–17789.

5. Phelan, D., Long, X., Xie, Y., Ye, Z.G., Glazer, A.M., Yokota, H., et al. Single crystal study of competing rhombohedral and monoclinic order in lead zirconate titanate. *Physical Review Letters* 2010;**105**:1–4.
6. Frantti, J., Ivanov, S., Eriksson, S., Rundlöf, H., Lantto, V., Lappalainen, J., et al. Phase transitions of $\text{pbzr}_x\text{ti}_{1-x}\text{o}_3$ ceramics. *Physical Review B* 2002;**66**:064108–15.
7. Bogdanov, A., Mysovsky, A., Pickard, C.J., Kimmel, A.V.. Modelling the structure of zr-rich $\text{pb}(\text{zr}_{1-x}\text{ti}_x)\text{o}_3$, $x=0.4$ by a multiphase approach. *Physical Chemistry Chemical Physics* 2016;**18**:28316.
8. Scott, J., Paz de Araujo, C.. Ferroelectric memories. *Science* 1989;**246**:1400–1405.
9. Catalan, G., Seidel, J., Ramesh, R., Scott, J.. Domain wall nanoelectronics. *Reviews of Modern Physics* 2012;**84**:119–156.
10. Lazarus, K.B., Crawley, E.F., Bohlmann, J.D., Worth, F.. Static aeroelastic control using strain actuated adaptive structures. *Journal of Intelligent Material Systems and Structures* 1991;**2**:386–440.
11. Zhao, Y.H., Hu, H.Y.. Active control of vertical tail buffeting by piezoelectric actuators. *Journal of Aircraft* 2009;**46**:1167–1175.
12. Jänker, P., Claeysen, F., Leletty, R., Sosniki, O., Pages, A., Magnac, G., et al. New actuators for aircraft , space and military applications. *Actuator 2010, 12th International Conference on New Actuators* 2008;:346.
13. Hooker, M.W.. Properties of pzt-based piezoelectric ceramics between -150 and 250 c. *Lockheed Martin Engineering Sciences Company* 1998;(NASA/CR-1998-208708):1–25.
14. Todorov, I.T., Smith, W., Trachenko, K., Dove, M.T.. Dlpoly3: new dimensions in molecular dynamics simulations via massive parallelism. *Journal of Materials Chemistry* 2006;**16**:1911–1918.
15. Mitchel, P.J., Fincham, D.. Shell model simulations by adiabatic dynamics. *Journal of Physics: Condensed Matter* 1993;**5**:1031–1038.
16. Chapman, J.B.J., Kimmel, A.V., Duffy, D.M.. Novel high-temperature ferroelectric domain morphology in pbtio_3 ultrathin films. *Physical Chemistry Chemical Physics* 2017;**19**:4243–4250.

17. Sepliarsky, M., Cohen, R.E.. First-principles based atomistic modeling of phase stability in pmn-xpt. *Journal of Physics: Condensed Matter* 2011;**23**:435902–11.
18. Wooldridge, J., Ryding, S., Brown, S., Burnett, T.L., Cain, M.G., Cernik, R., et al. Simultaneous measurement of x-ray diffraction and ferroelectric polarization data as a function of applied electric field and frequency. *Journal of Synchrotron Radiation* 2012; **19**:710–716.
19. Wang, D., Fotinich, Y., Carman, G.P.. Influence of temperature on the electromechanical and fatigue behavior of piezoelectric ceramics. *Journal of Applied Physics* 1998; **83**:5342–5350.
20. Xu, R., Liu, S., Grinberg, I., Karthik, J., Damodaran, A.R., Rappe, A.M., et al. Ferroelectric polarization reversal via successive ferroelastic transitions. *Nature materials* 2015;**14**:79–86.
21. Yan, F., Xing, G.Z., Li, L.. Low temperature dependent ferroelectric resistive switching in epitaxial bifeo3 films. *Applied Physics Letters* 2014;**104**:13–17.
22. Jiang, A., Dawber, M., Scott, J.F., Wang, C., Migliorato, P., Gregg, M.. Studies of switching kinetics in ferroelectric thin films. *Japanese Journal of Applied Physics* 2003; **42**:6973–6982.
23. Hu, W.J., Juo, D.M., You, L., Wang, J., Chen, Y.C., Chu, Y.H., et al. Universal ferroelectric switching dynamics of vinylidene fluoride-trifluoroethylene copolymer films. *Scientific Reports* 2014;**4**:47728.
24. Chapman, J.B.J., Cohen, R.E., Kimmel, A.V., Duffy, D.M.. Improving the Functional Control of Aged Ferroelectrics using Insights from Atomistic Modelling. *ArXiv e-prints* 2017;1705.09709.
25. Zeng, X., Cohen, R.E.. Thermo-electromechanical response of a ferroelectric perovskite from molecular dynamics simulations. *Applied Physics Letters* 2011;**99**:142902–3.
26. Sai, N., Rabe, K.M., Vanderbilt, D.. Theory of structural response to macroscopic electric fields in ferroelectric systems. *Physical Review B* 2002;**66**:104108.
27. Poykko, S., Chadi, D.J.. Ab initio study of 180 degree domain wall energy and structure in pbtio3. *Applied Physics Letters* 1999;**75**:2830–2832.

28. Beckman, S.P., Wang, X., Rabe, K.M., Vanderbilt, D.. Ideal barriers to polarization reversal and domain-wall motion in strained ferroelectric thin films. *Physical Review B* 2009;**79**:1–8.
29. Shimada, T., Wakahara, K., Umeno, Y., Kitamura, T.. Shell model potential for PbTiO_3 and its applicability to surfaces and domain walls. *Journal of Physics: Condensed Matter* 2008;**20**:325225.
30. Stemmer, S., Streiffer, S.K., Ernst, F., Rühle, M.. Atomistic structure of 90-degree domain-walls in ferroelectric PbTiO_3 thin-films. *Philosophical Magazine A* 1995;**71**:713–724.
31. Shin, Y.H., Grinberg, I., Chen, I.W., Rappe, A.M.. Nucleation and growth mechanism of ferroelectric domain-wall motion. *Nature* 2007;**449**:881–884.
32. Guo, R., Cross, L.E., Park, S.E., Noheda, B., Cox, D.E., Shirane, G.. Origin of the high piezoelectric effect response in $\text{PbZr}_{1-x}\text{Ti}_x\text{O}_3$. *Physical Review Letters* 2000;**84**:5423–5426.
33. Geneste, G.. Correlations and local order parameter in the paraelectric phase of barium titanate. *Journal of Physics: Condensed Matter* 2011;**23**:125901–16.
34. Qi, Y., Liu, S., Grinberg, I., Rappe, A.. Atomistic description for temperature-driven phase transitions in BaTiO_3 . *Physical Review B* 2016;**94**:134308–8.
35. Jo, J.Y., Han, H.S., Yoon, J.G., Song, T.K., Kim, S.H., Noh, T.W.. Domain switching kinetics in disordered ferroelectric thin films. *Physical Review Letters* 2007;**99**:1–4.
36. Kamel, T.M., de With, G.. Double-peak switching current in soft ferroelectric lead zirconate titanate. *Journal of Applied Physics* 2007;**102**:044118–5.
37. Stolichnov, I., Tagantsev, A., Setter, N., Cross, J.S., Tsukada, M.. Crossover between nucleation-controlled kinetics and domain wall motion kinetics of polarization reversal in ferroelectric films. *Applied Physics Letters* 2003;**83**:3362–3364.
38. Vopsaroiu, M., Blackburn, J., Cain, M.G., Weaver, P.. Thermally activated switching kinetics in second-order phase transition ferroelectrics. *Physical Review B* 2010;**82**:024109–10.
39. Tagantsev, A., Stolichnov, I., Setter, N., Cross, J., Tsukada, M.. Non-kolmogorov-avrami switching kinetics in ferroelectric thin films. *Physical Review B* 2002;**66**:214109–6.